
Proceedings Paper:
Forrester, J., Davidson, J. orcid.org/0000-0002-6576-3995 and Foster, M. (2023) Bidirectional inverting piezo resonator-based (BIPR) converter for cell balancing applications. In: 2023 IEEE Energy Conversion Congress and Exposition (ECCE) Proceedings. 2023 IEEE Energy Conversion Congress and Exposition (ECCE), 29 Oct - 02 Nov 2023, Nashville, Tennessee. USA. Institute of Electrical and Electronics Engineers (IEEE) , pp. 195-201. ISBN 9798350316452

https://doi.org/10.1109/ECCE53617.2023.10362516

Bidirectional inverting piezo resonator-based (BIPR) converter for cell balancing applications

Jack Forrester
Department of Electronic and Electrical Engineering
University of Sheffield
Sheffield, UK
jack.forrester@sheffield.ac.uk

Jonathan Davidson
Department of Electronic and Electrical Engineering
University of Sheffield
Sheffield, UK
jonathan.davidson@sheffield.ac.uk

Martin Foster
Department of Electronic and Electrical Engineering
University of Sheffield
Sheffield, UK
m.p.foster@sheffield.ac.uk

***Abstract*—A novel piezo resonator-based resonant converter topology is presented, specifically tailored for active cell balancing applications. The bidirectional operation of the converter is presented, and the control requirements are discussed. Simulations are performed to determine the output voltage gain and output current of the converter. Finally, the cell balancing performance of the converter is simulated and compared to a passive balancing method, showing improved efficiency and balancing speed.**

Keywords—DC-DC converters, Battery Management Systems (BMS), Piezoelectric resonator

I. Introduction

Cell balancing is one of many critical functions of battery management systems (BMS), ensuring the state of charge (SOC) of each cell within a string is equalized, increasing the performance of the battery [1]. Passive approaches typically dissipate charge from high SOC cells, reducing their SOC until it reaches that of the lowest SOC cell in the battery [2]. Active methods use additional circuitry to transfer charge from high SOC cells to low SOC cells [2]. Active approaches are more efficient than passive methods but are difficult to implement and are typically larger in volume. As a result, commercial BMS integrated circuits focus on the use of passive balancing rather than active balancing. However, several active balancing approaches have been previously presented including, switched capacitor [3], [4], Ćuk converter, buck-boost converter, flyback converter, quasi-resonant converter, and transformer based [2].

Piezoelectric resonators (PRs) and piezoelectric transformers (PTs) use the piezoelectric effect to convert energy between electrical and mechanical domains. Both devices are commonly integrated into resonant power converters where they replace the discrete passive components. PRs and PTs both exhibit high Q factor resonant tank circuits, giving rise to highly efficient, compact resonant converters for low power (<50W) applications [5], [6]. PTs have seen more academic interest than PRs [7]–[10], given the ideal transformer they contain within their equivalent circuit, as shown in Fig. 1. This allows both isolation and a turns ratio to be achieved. However, whilst zero-voltage switching (ZVS) can be achieved in PT based converters without additional passive components, achieving ZVS whilst having appropriate control of the output voltage is challenging due to the narrow operating frequency range [11]–[13]. As a result, PR converters are of greater academic interest, as although they do not provide galvanic isolation, PRs are versatile with authors presenting PR based resonant converter topologies for various output power and voltage gain requirements [14]–[17].

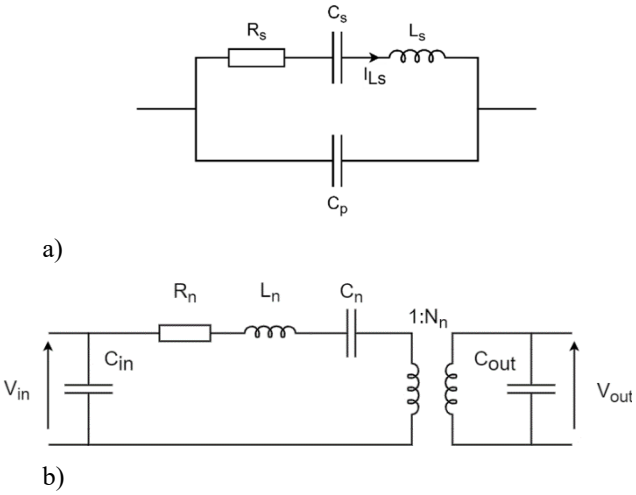

Fig. 1. Equivalent circuit for a) piezoelectic resonator (PR) b) piezoelectric transformer (PT)

We present a novel PR based converter which can be used in both step-up and step-down applications, can be operated bidirectionally and inverts the polarity of the output voltage. These properties make the bidirectional inverting piezo-resonator (BIPR) converter ideal for use in active cell balancing applications. The BIPR converter has reduced component count, manufacturing complexity and size compared to typical active balancing approaches.

II. Active Cell Balancing Requirements

A number of active cell balancing schemes exist, these include: cell-to-cell (energy is transferred between adjacent cells in the string), cell-to-pack (energy is transferred from a high-SOC cell to the whole pack) and pack-to-cell (energy is extracted from the whole pack and provided to a low-SOC cell) [18]. In this work, a cell-to-cell scheme will be used. In our implementation, a converter is placed between each pair of adjacent cells in the string, where the converter allows charge to be passed between the adjacent cells, as shown in Fig. 2. In Fig. 2, cells A and D are assumed to have a high SOC and cells B and C have a low SOC.

To allow energy transfer, the balancing converter has several requirements. Firstly, it must be able to support bidirectional energy transfer, so that energy can be transferred both up and down the string of cells. The converter must invert the polarity of the output voltage compared to the input voltage. This feature is required as a

local common exists between each adjacent pair of cells, therefore the voltage on the top cell is observed by the converter as positive and the voltage on the bottom cell is observed as negative. Therefore, to allow energy to be passed between the cells, the converter must accept a positive input voltage and output a negative voltage (and vice versa). This leads to another key requirement: the converter must be able to operate with the input voltage level as low as a single cell with a gain both above and below unity. This is important as the converter is only required to operate with a gain of less than unity but for some converter topologies this requires duty cycles close to the theoretical limits. As a result, the controller has limited regulation and, in some cases due to parasitic components, the converter will not operate correctly.

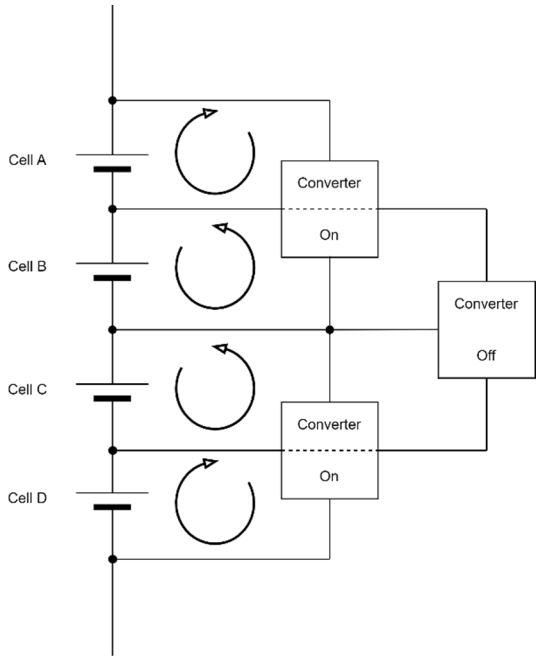

Fig. 2. Active cell balancing network during operation, with circular arrows showing the flow of current

III. Bidirectional Inverting Piezo Resonator-Based (BIPR) Converter

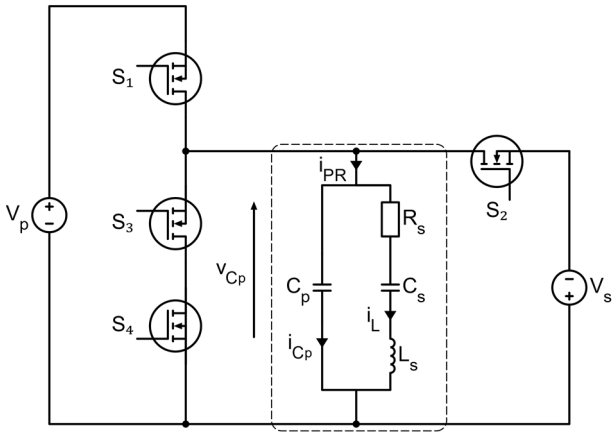

Fig. 3. BIPR converter, dashed box shows PR equivalent circuit

The BIPR converter is proposed for use in active cell balancing applications. This converter exhibits both bidirectional energy transfer capabilities and output voltage inversion, making it ideal for this application. Fig. 3 shows the proposed BIPR converter, with the dashed box highlighting the equivalent circuit of the PR. In a practical application, V_p and V_s represent two adjacent series connected cells within a battery. Switches S_1 - S_4 are MOSFETs, with switches S_3 and S_4 forming a bidirectional switch. S_3 can be replaced with a diode for easier gate drive requirements.

A. Operation of BIPR converter

The BIPR converter's operation can be described by six operating modes, which depend on the conduction states of the MOSFET switches. As the BIPR converter supports bidirectional energy transfer, a different set of operating modes are required for converter operation in each direction.

1) Primary-to-secondary (P-to-S) energy transfer

In P-to-S energy transfer, the BIPR converter will operate with a positive input voltage and a negative output voltage. This is used to transfer charge from a high-SOC cell to the cell below it in the string, such as between cells A and B in Fig. 2.

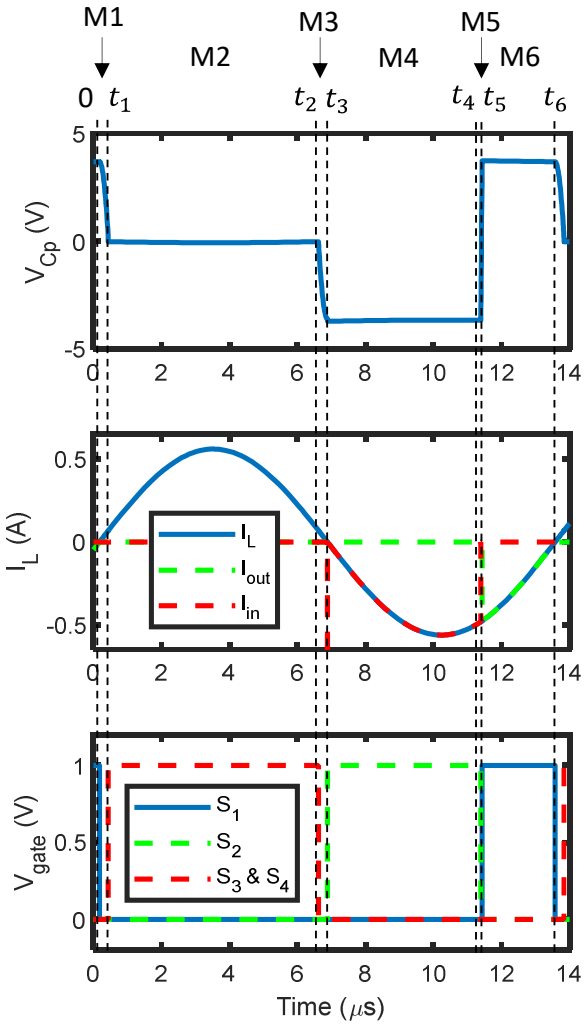

Fig. 4. PR voltage, resonant current and gate drive waveforms for the BIPR operating with V_p = 3.7V and V_s = -3.7V in P-to-S energy transfer

Fig. 4 shows voltage and current waveforms for the BIPR converter when operating with primary to secondary energy transfer (i.e. forward transfer with positive input).

This operation is described by the following six operating modes:

M1 $(0 \rightarrow t_1)$: At $t = 0$, the PR voltage (V_{Cp}) is equal to V_p and the resonant current crosses zero. S_1 turns on with ZVS and current flows from V_p to the resonator, energising the resonator.

M2 $(t_1 \rightarrow t_2)$: At $t = t_1$, S_1 turns off and resonant current i_L discharges C_p from V_p to V_s

M3 $(t_2 \rightarrow t_3)$: At $t = t_2$, S_2 turns on with ZVS and i_L flows to the output V_s through S_2

M4 $(t_3 \rightarrow t_4)$: At $t = t_3$ the resonant current i_L crosses zero, S_2 turns off and the resonant current charges C_p from V_s to 0

M5 $(t_4 \rightarrow t_5)$: At $t = t_4$, S_3 and S_4 turn on with ZVS, clamping PR voltage to 0.

M6 $(t_5 \rightarrow t_6)$: At $t = t_5$, S_3 and S_4 both turn off and i_L charges C_p from 0 to V_p

2) Secondary-to-primary (S-to-P) energy transfer

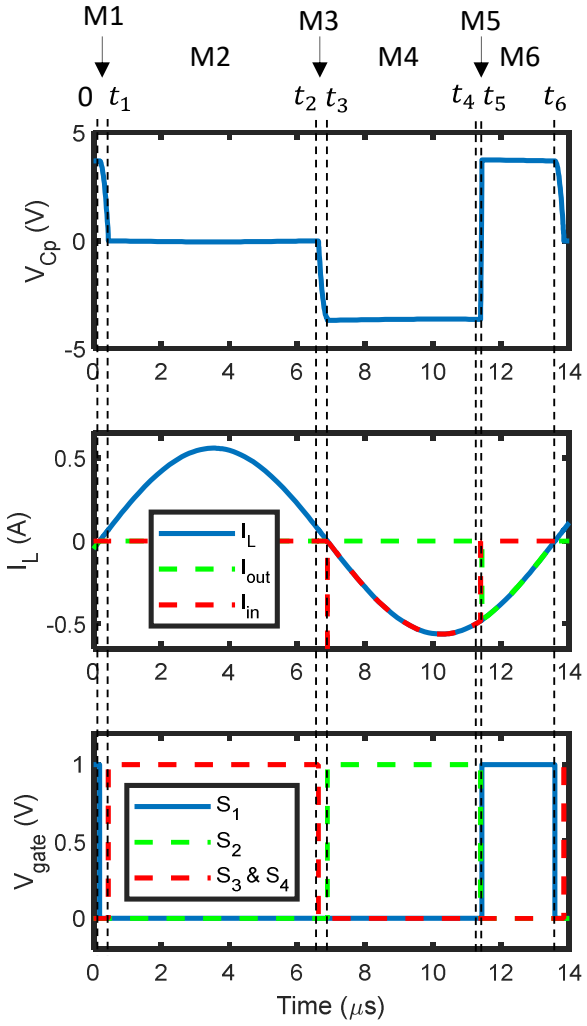

Fig. 5. PR voltage, resonant current and gate drive waveforms for the BIPR operating with V_p = 3.7V and V_s = -3.7V in S-to-P energy transfer

In S-to-P energy transfer, the BIPR converter will operate with a negative input voltage and a positive output voltage. This is used to transfer charge from a high SOC cell to the cell above it in the string, such as between cells C and D in Fig. 2.

Fig. 5 shows idealized voltage and current waveforms for the BIPR converter when operating with secondary to primary energy transfer (i.e. reverse transfer with negative input). This operation is described by the following six operating modes:

M1 $(0 \rightarrow t_1)$: At $t = 0$, the PR voltage (V_{Cp}) is equal to the output voltage V_p and the resonant current i_L undergoes a positive zero crossing. All switches are turned off, so i_L flows into C_p, discharging it to 0.

M2 $(t_1 \rightarrow t_2)$: At $t = t_1$, S_3 and S_4 turn on with ZVS, clamping PR voltage to 0.

M3 $(t_2 \rightarrow t_3)$: At $t = t_2$, S_3 and S_4 both turn off and i_L discharges C_p from 0 to V_s

M4 $(t_3 \rightarrow t_4)$: At $t = t_3$ the resonant current i_L undergoes a negative zero crossing, S_2 turns on and current flows from V_s to the resonator, charging the resonator.

M5 $(t_4 \rightarrow t_5)$: At $t = t_4$, S_2 turns off and i_L charges C_p from V_s to V_p

M6 $(t_5 \rightarrow t_6)$: At $t = t_5$, S_1 turns on and i_L flows to the output V_p through S_1

3) BIPR converter control

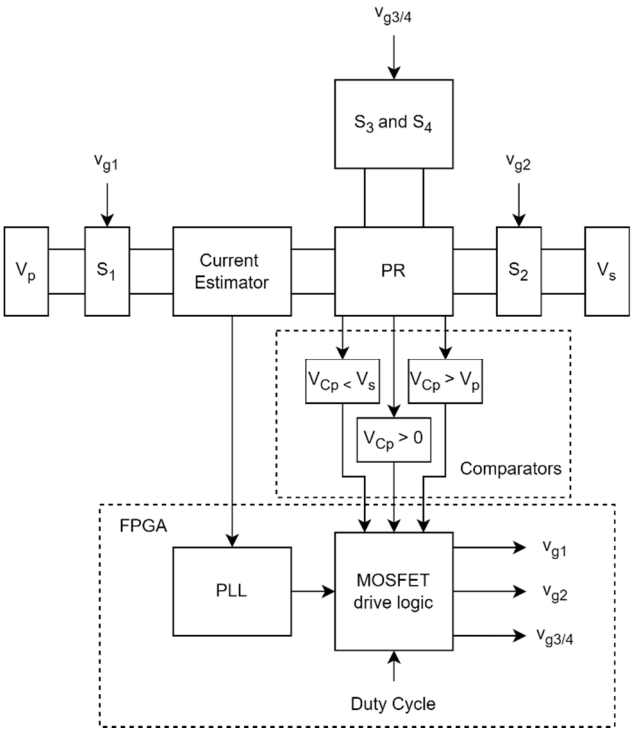

Fig. 6. Block diagram for an example BIPR converter controller

A block diagram of a sample controller for the BIPR converter is presented in Fig. 6. Each converter is operated at its system resonant frequency, i.e. the frequency which ensures the driving signals are in phase with the resonant current. However, in piezoelectric based converters, the resonant current cannot be directly measured as it is not a

measurable current but is a modelling analogue of the vibration velocity. Discounting the use of a laser vibrometer, the resonant current can only be estimated; this is standard practice for PR and PT converters [19], [20].

The mode timings are tightly controlled, to both control the output current and to ensure ZVS. In P-to-S conversion, the duration of M1 is set, either manually (in open loop control) or by a controller (closed loop control) to control the output current, with a larger M1 duty cycle giving a larger output current. Modes M3 and M5 begin based on when the v_{C_p} voltage equals v_s and 0 respectively. Therefore, this voltage needs to be an input to the controller, this can be achieved using either a comparator (for analogue or digital control) or ADC (for digital control). Finally, M5 should end with just sufficient time for C_p to charge to V_p before the end of the cycle.

Similarly, for S-to-P conversion, the duration of M4 controls the output current. Modes M2 and M6 start when the v_{C_p} voltage equals 0 and V_p respectively. Finally, and in similarity to the P-to-S case, M2 should end with just sufficient time for C_p to discharge to 0 before resonant current zero crossing.

Additionally, in a cell balancing application, control of the whole network of converters is required in order to balance the full string of cells. Therefore, a control algorithm is required to determine which of the converters connected to the battery should be in operation at any time, should energy be transferred P-to-S or S-to-P in each converter and a suitable balancing current for each converter. Determining a suitable control algorithm is a challenging task for cell-to-cell balancing networks, especially in the worst-case scenario of the highest SOC cell and the lowest SOC cell being at opposite ends of the battery, requiring charge to be transferred through the whole battery of cells to achieve balance. Implementing and compensating a controller for the BIPR converter and BMS integration is beyond the scope of this work.

IV. Simulation

A. Converter operation

Initially, the operation of the converter will be examined with a resistive load and then with a cell as a load. In both cases a Steminc SMD30T21F1000S radially vibrating piezoresonator (Fig. 7) is used, with its equivalent circuit properties given in TABLE I. Simulations will be performed using LTSpice.

Fig. 7. SMD30T21F1000S piezo resonator

TABLE I. SMD30T21F1000S PR equivalent circuit properties

R_s (Ω)	L_s (mH)	C_s (nF)	C_p (nF)
2.22	4.47	1.02	2.54

A resistive load is used to examine the output voltage gain that can be achieved using the BIPR converter. A 50 Ω and a 500 Ω load are used, and the duty cycle (M1 for P-to-S and M4 for S-to-P) is varied through a range of 15-40%, for both directions of energy transfer. The output voltage gain is observed for each variation. Idealised switches are used, with an on-state resistance of 0.1Ω. It should be noted that no parasitic capacitance is simulated for the switches as this has a negligible effect on performance due to the large parallel capacitance of the PR. The results are shown in Fig. 8.

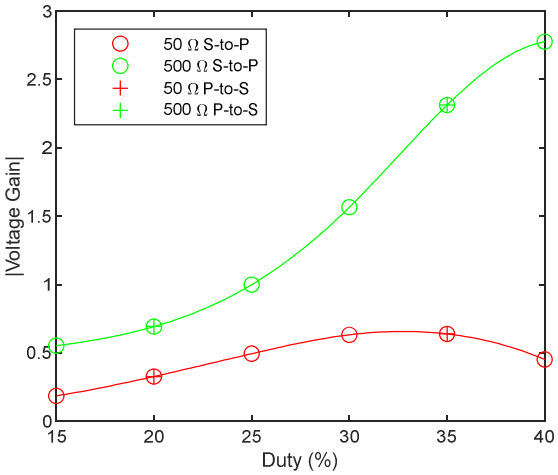

Fig. 8. Voltage gain against M1 duty (for P-to-S mode) and M4 duty (for S-to-P mode) with both a 50Ω and 500Ω load

From Fig. 8 we can conclude that the converter exhibits the same gain irrespective of the direction of energy transfer. During operation with the 50Ω load, the gain of the converter is lower than 1 for all variations in duty cycle. This is due to the large output current that is generated for this load and as a result, the high level of power loss in the resonator. For a less lossy resonator, higher gain could have been achieved. With a load of 500Ω, the converter is able to achieve a wide range of gains from 0.5 to 2.75, showing the versatility of the converter.

A second simulation was performed to observe the output current that is achieved when the converter is used in a cell balancing application. In this case, the resistive load is replaced with a voltage source (modelling a cell), with both the input voltage and output voltage set to 3.7V, the nominal voltage of a single Li-ion cell. Similar to the previous simulation, the M4 duty cycle is varied between 25 and 40%, and the output current is observed when operated in S-to-P mode (again operation is the same in P-to-S mode). In addition, a second, lower loss PR presented by Pollet et al [17] is simulated, with properties given in TABLE II. The results of these simulations are shown in Fig. 9.

TABLE II. POLLET ET AL [13] PR EQUIVALENT CIRCUIT PROPERTIES

R_s (Ω)	L_s (mH)	C_s (nF)	C_p (nF)
0.6	1.1	2.9	8.4

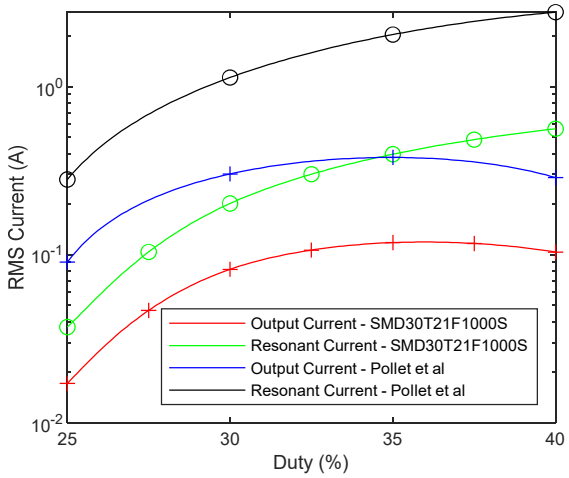

Fig. 9. Output and resonant current with changes in gain controlling duty cycle, for both the SMD30T21F1000S and PR in [17], with V_p = 3.7V and V_s = -3.7V in S-to-P energy transfer

Fig. 9 shows the output current of the converter can be controlled by the duty cycle (M1 or M4 depending on energy transfer direction), in agreement with theory. In both cases, the maximum output current is achieved at around 35% duty, with higher duty giving higher loss and thus lower output current. The duty cycle control over output current gives the BMS control over the balancing current (compared to passive balancing) and thus more granular control over balancing the cells. A maximum current of 120mA$_{RMS}$ is observed with the SMD30T21F1000S PR and a maximum of 380mA$_{RMS}$ for the PR presented in [17]. In comparison, the BQ79616 battery monitor and balancing IC from Texas Instruments (passive balancing), exhibits a balancing current of 240mA DC, thus with balancing current in between the two simulated BIPR converters. The BIPR converter only achieves an efficiency between 10-84% (using the PR in [17]), which, although comparatively low compared to other techniques, is more efficient than the passive method.

B. BIPR converter cell balancing

To evaluate the performance of the BIPR converter in a cell balancing application, a simplified simulation was performed. Due to the sub microsecond-level of control required to operate the BIPR converter (1% change in duty at 89kHz equals a change of 112ns) and the long simulation duration required to observe the cell balancing performance, the converter will be replaced by two behavioural current sources to enable accurate and timely cell balancing simulation. Here an S-to-P energy transfer scenario was simulated, with a 2-cell Li-ion battery (Cell A SOC of 65%, Cell B SOC of 70%), each with a capacity of 0.25Ah, as shown in Fig. 10. Balancing will be simulated during charging of the battery at a constant current of 1C (i.e. 0.25 A). Both the BIPR converter and a passive balancing network are simulated to observe the differences.

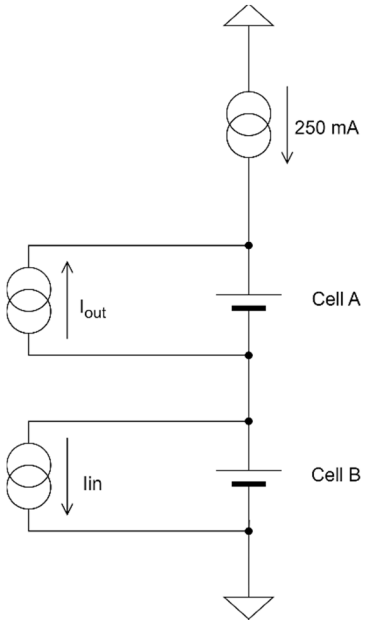

Fig. 10. Simulated BIPR converter cell balancing circuit

To simulate the BIPR converter, a suitable input and output current shape and amplitude should be determined. Observing Fig. 5, with a M4 duty cycle of 30%, we can see that the resonant current is drawn from the negative cell (I_{in}) for 30% of the cycle ($t_3 \rightarrow t_4$), then following a short (we assume negligible) period of time where the resonant current charges C_p to V_p ($t_4 \rightarrow t_5$), the resonant current is then transferred into the positive cell (I_{out}) for the remaining ~20% of the cycle ($t_5 \rightarrow t_6$). To simulate this behaviour, a multiplication block was used in Simulink, multiplying a sine source (set to an amplitude of 1.13A and a frequency of 89kHz to match the resonant current found in Fig. 9, for a 30% duty and using for the PR in [17]) with the gate signal for switches S_1 and S_2, allowing two signals to be produced which equal i_{in} and i_{out} in Fig. 5. Therefore, i_{in} and i_{out} in Fig. 10 are set equal to these signals. To simulate the battery, the Specialized Power Systems library in Simulink was used and a 0.25Ah Li-Ion cell was simulated with an internal resistance of 0.148 Ω. The circuit was connected as shown in Fig. 10. For passive balancing, a constant current sink was used and set to draw 240mA from Cell B, until balanced.

The set-up was simulated with a duration time of 200s for both the equivalent BIPR converter and passive balancing circuits. Fig. 11 shows results of this simulation, showing the SOC of both cells, for both passive and BIPR balancing techniques.

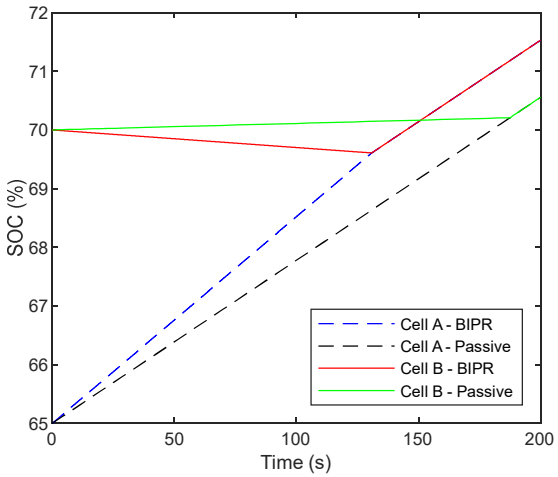

Fig. 11. SOC for both cells over time for both the BIPR and passive balancing circuits

As can be seen in Fig. 11, the BIPR converter achieves faster balancing than the passive balancing technique. This increase in balancing speed is due to several reasons: first, the larger current drawn from Cell B, leading to a reduction in SOC in Cell B. Secondly, in the BIPR converter case, as the charge drawn from Cell B is transferred to the Cell A, this causes an increase the charging speed of Cell A compared to the passive balancing case. The increase in balancing speed also allows faster charging of the battery, with both cells exhibiting 71.5% SOC compared to 70.5% SOC in the passive case after 200s, for the same charging current. Finally, due to the transfer of excess charge (rather than dissipation) from Cell B to the Cell A, the BIPR converter is significantly more efficient than the passive case.

V. Component Selection

For the proposed converter, the chosen PR should exhibit low losses, to maximise output (balancing) current and for high efficiency. To the authors' knowledge, it is not possible to accurately predict PR loss as the loss arises from several sources, which include the piezoelectric material, quality of PR construction, electrode connection location, mounting method, and varies with ambient temperature [21]. However, constructing a PR using a 'hard' piezoelectric material with a high coupling factor for the chosen vibration mode and a high Q factor should help to minimise the losses. For a radial resonator (such as that used in this work), the radius of the PR determines the resonant frequency, and therefore should be chosen to give a suitable resonant frequency of the given application. Finally, the thickness of the resonator controls the parallel capacitance, this should be minimised in most cases to minimise the time where energy is circulating in the PR and to make achieving ZVS easier [22].

Assuming ZVS is achieved in the BIPR converter, the choice of MOSFET should be based around minimising $R_{\mathrm{DS_{on}}}$, to maximise converter efficiency. Minimising MOSFET parasitic capacitance is of lower importance due to the relatively high PR parallel capacitance. It should also be noted that switch S_3 can be replaced with a low loss, fast recovery diode for easier gate drive requirements but this will result in higher losses and lower overall efficiency.

VI. Conclusion

A new PR based converter is presented for cell balancing applications. The operation of the BIPR converter is described for bidirectional energy transfer. A series of simulations are presented showing the good performance of the BIPR converter compared to passive balancing techniques. The choice of PR and additional circuit components are discussed.

VII. Referecnes

[1] M. Kamel, V. Sankaranarayanan, R. Zane, and D. Maksimović, 'State-of-Charge Balancing With Parallel and Series Output Connected Battery Power Modules', *IEEE Trans. Power Electron.*, vol. 37, no. 6, pp. 6669–6677, Jun. 2022, doi: 10.1109/TPEL.2022.3143835.

[2] J. Carter, Z. Fan, and J. Cao, 'Cell equalisation circuits: A review', *J. Power Sources*, vol. 448, p. 227489, Feb. 2020, doi: 10.1016/j.jpowsour.2019.227489.

[3] C. Pascual and P. T. Krein, 'Switched capacitor system for automatic series battery equalization', in *Proceedings of APEC 97 - Applied Power Electronics Conference*, Feb. 1997, pp. 848–854 vol.2. doi: 10.1109/APEC.1997.575744.

[4] Y. Ye, K. W. E. Cheng, Y. C. Fong, X. Xue, and J. Lin, 'Topology, Modeling, and Design of Switched-Capacitor-Based Cell Balancing Systems and Their Balancing Exploration', *IEEE Trans. Power Electron.*, vol. 32, no. 6, pp. 4444–4454, Jun. 2017, doi: 10.1109/TPEL.2016.2584925.

[5] A. V. Carazo, '50 years of piezoelectric transformers. Trends in the technology', *MRS Online Proc. Libr. Arch.*, vol. 785, 2003.

[6] Y.-P. Liu, D. Vasic, F. Costa, and D. Schwander, 'Piezoelectric 10W DC/DC converter for space applications', in *Proceedings of the 2011 14th European Conference on Power Electronics and Applications*, Aug. 2011, pp. 1–7.

[7] J. Forrester, J. N. Davidson, M. P. Foster, and D. A. Stone, 'Circuit Simulator Compatible Model for the Ring-Dot Piezoelectric Transformer', *J. Microelectromechanical Syst.*, vol. 32, no. 1, pp. 103–116, Feb. 2023, doi: 10.1109/JMEMS.2022.3220042.

[8] Y. Hou *et al.*, 'Vertically Stacked Piezoelectric Transformer for High-Frequency Power Amplifier', in *2023 IEEE Applied Power Electronics Conference and Exposition (APEC)*, Mar. 2023, pp. 392–396. doi: 10.1109/APEC43580.2023.10131481.

[9] J. Randrianarivelo, F. E. Ratolojanahary, M. Rguiti, D. Jeannot, L. Elmaimouni, and I. Naciri, 'Modeling and Analysis of Transverse-Type Piezoelectric Transformer By Means of a Polynomial Approach', in *2022 IEEE 7th Southern Power Electronics Conference (SPEC)*, Dec. 2022, pp. 1–6. doi: 10.1109/SPEC55080.2022.10058212.

[10] Z. Yang, J. Forrester, J. N. Davidson, M. P. Foster, and D. A. Stone, 'Critical design criterion for inductorless H-bridge driven piezoelectric-transformer-based power supplies', in *IECON 2022 – 48th Annual Conference of the IEEE Industrial Electronics Society*, Oct. 2022, pp. 1–6. doi: 10.1109/IECON49645.2022.9968767.

[11] Z. Yang, J. N. Davidson, and M. P. Foster, 'Output voltage regulation for piezoelectric transformer-based resonant power supplies using phase-locked loop', in *The 10th International Conference on Power Electronics, Machines and Drives (PEMD 2020)*, Dec. 2020, pp. 455–460. doi: 10.1049/icp.2021.1099.

[12] M. Khanna, R. Burgos, Q. Wang, K. D. T. Ngo, and A. V. Carazo, 'New Tunable Piezoelectric Transformers and Their Application in DC-DC Converters', *IEEE Trans. Power Electron.*, vol. 32, no. 12, pp. 8974–8978, Dec. 2017, doi: 10.1109/TPEL.2017.2702124.

[13] M. P. Foster, J. N. Davidson, E. L. Horsley, and D. A. Stone, 'Critical Design Criterion for Achieving Zero Voltage Switching in Inductorless Half-Bridge-Driven Piezoelectric-Transformer-Based Power Supplies', *IEEE Trans. Power Electron.*, vol. 31, no. 7, pp. 5057–5066, Jul. 2016, doi: 10.1109/TPEL.2015.2481706.

[14] J. D. Boles, J. J. Piel, and D. J. Perreault, 'Enumeration and Analysis of DC–DC Converter Implementations Based on Piezoelectric

Resonators', *IEEE Trans. Power Electron.*, vol. 36, no. 1, pp. 129–145, Jan. 2021, doi: 10.1109/TPEL.2020.3004147.

[15] M. Touhami, G. Despesse, and F. Costa, 'A New Topology of DC–DC Converter Based on Piezoelectric Resonator', *IEEE Trans. Power Electron.*, vol. 37, no. 6, pp. 6986–7000, Jun. 2022, doi: 10.1109/TPEL.2022.3142997.

[16] V. Breton, E. Bigot, G. Despesse, and F. Costa, 'A New Isolated Topology of DC–DC Converter Based on Piezoelectric Resonators', *IEEE Trans. Power Electron.*, vol. 38, no. 8, pp. 10012–10025, Aug. 2023, doi: 10.1109/TPEL.2023.3276478.

[17] B. Pollet, F. Costa, and G. Despesse, 'A new inductorless DC-DC piezoelectric flyback converter', in *2018 IEEE International Conference on Industrial Technology (ICIT)*, Feb. 2018, pp. 585–590. doi: 10.1109/ICIT.2018.8352243.

[18] J. Gallardo-Lozano, E. Romero-Cadaval, M. I. Milanes-Montero, and M. A. Guerrero-Martinez, 'Battery equalization active methods', *J. Power Sources*, vol. 246, pp. 934–949, Jan. 2014, doi: 10.1016/j.jpowsour.2013.08.026.

[19] Z. Yang, J. Forrester, J. N. Davidson, M. P. Foster, and D. A. Stone, 'Resonant Current Estimation and Phase-Locked Loop Feedback Design for Piezoelectric Transformer-Based Power Supplies', *IEEE Trans. Power Electron.*, vol. 35, no. 10, pp. 10466–10476, Oct. 2020, doi: 10.1109/TPEL.2020.2976206.

[20] J. Forrester, M. Foster, and J. Davidson, 'Resonant current estimation and phase-locked loop control system for inductorless step-up single piezo element-based (SUPRC) DC-DC converter', presented at the 48th Annual Conference of the Industrial Electronics Society IECON 2022 Conference, Brussels, Belgium, Oct. 2022.

[21] J. Forrester *et al.*, 'Comparison of BSPT and PZT Piezoelectric Ceramic Transformers for High-Temperature Power Supplies', *Adv. Eng. Mater.*, p. 2200513, Sep. 2022, doi: 10.1002/adem.202200513.

[22] J. Forrester, J. N. Davidson, and M. P. Foster, 'Inductorless Step-up Piezoelectric Resonator (SUPR) Converter: a Describing Function Analysis', *IEEE Trans. Power Electron.*, pp. 1–13, 2023, doi: 10.1109/TPEL.2023.3294802.